energies

MDPI

Quantitative Analysis of the Sensitivity of UHF Sensor Positions on a 420 kV Power Transformer Based on Electromagnetic Simulation

Chandra Prakash Beura [1,*], Michael Beltle [1], Stefan Tenbohlen [1] and Martin Siegel [2]

[1] Institute of Power Transmission and High Voltage Technology (IEH), University of Stuttgart, 70569 Stuttgart, Germany; michael.beltle@ieh.uni-stuttgart.de (M.B.); stefan.tenbohlen@ieh.uni-stuttgart.de (S.T.)

[2] BSS Hochspannungstechnik GmbH, 71229 Leonberg, Germany; martin.siegel@bss-hs.de

* Correspondence: chandra.beura@ieh.uni-stuttgart.de

Received: 25 November 2019; Accepted: 16 December 2019; Published: 18 December 2019

Abstract: With an increasing interest in ultra-high frequency (UHF) partial discharge (PD) measurements for the continuous monitoring of power transformers, it is necessary to know where to place the UHF sensors on the tank wall. Placing a sensor in an area with many obstructions may lead to a decrease in sensitivity to the UHF signals. In this contribution, a previously validated simulation model of a three-phase 300 MVA, 420 kV power transformer is used to perform a sensitivity analysis to determine the most sensitive sensor positions on the tank wall when PD activity occurs inside the windings. A matrix of UHF sensors located on the transformer tank is used to perform the sensitivity analysis. Some of the windings are designed as layer windings, thus preventing the UHF signals from traveling through them and creating a realistic situation with very indirect propagation from source to sensor. Based on these findings, sensor configurations optimized for UHF signal sensitivity, which is also required for PD source localization, are recommended for localization purposes. Additionally, the propagation and attenuation of the UHF signals inside the windings and the tank are discussed in both oil and air.

Keywords: power transformers; partial discharge; PD; UHF; monitoring; acceptance tests; PD sensors; sensor positioning; sensitivity evaluation

1. Introduction

Since power transformers are vital components of electrical networks, their condition assessment is of utmost importance. Continuous undetected partial discharge (PD) activity can lead to complete failure of the equipment and hence, should be detected at an early stage. Ultra-high frequency (UHF) PD measurement employs UHF sensors that detect the propagating electromagnetic waves generated by PD activity in the range of 300 MHz to 3 GHz [1,2]. This method has the advantage of being resilient against external noise [3] and providing the possibility of three-dimensional PD source localization [4]. Recent developments have included different designs of UHF sensors [5–9], PD source localization algorithms [10,11], and a calibration proposal [12,13] so that the method can be introduced in addition to the IEC 60270 PD measurement [14] during transformer acceptance tests. Since UHF PD measurement requires the placement of UHF sensors at different positions on the transformer tank [9,15,16], it is required to analyze the sensitivity of various prospective sensor positions.

In an experiment performed on a three-phase 300 MVA, 420 kV grid coupling power transformer, holes were drilled at different points on the transformer tank, and monopole antennas

were installed [17]. These monopole antennas were used to transmit and receive artificial UHF signals generated by a pulse generator. Based on the attenuation of the UHF signals and consideration of electric field stress, certain positions were recommended for installing UHF sensors. However, the conclusions drawn were limited to the locations where holes were drilled in the tank. Additionally, since no artificial PD sources could be placed inside the windings, the propagation of the EM waves was mostly outside the windings, and the propagation from sources within the windings could not be analyzed [17].

Therefore, a three-dimensional finite element method (FEM) [18] simulation model of the investigated power transformer was developed in CST Microwave Studio and validated based on the experimental data. The validated model does not contain the on-load tap changer (OLTC) as its addition nearly doubled the number of mesh cells in the model, and the trade-off between computational time and accuracy of results was unfavorable [19].

In this investigation, using the simulation model, multiple artificial PD sources were placed in the windings, and an array of sensors were used to measure the signals from each source. Based on the maximum peak-to-peak voltage received by the sensors, the most sensitive sensor positions were identified, sensor configurations were recommended. Additionally, the difference in signal propagation and attenuation in two dielectric mediums (air and oil) were studied.

2. Simulation Setup

Each phase of the transformer consists of the following windings: LV, MV, HV, coarse, and fine windings. The LV, coarse, and fine windings are layer windings, which are modelled as solid cylinders. The MV and HV windings are disk windings. In such windings, the individual turns of each disk are not considered, and the spacing between two disks is 0.6 cm. The windings are modelled using copper as the material with a coating of oil-impregnated paper on top of the copper. The materials used for modelling the tank and the core are steel and silicon steel, respectively. The materials used in the construction of the model along with their properties (relative permittivity, electric conductivity, and relative magnetic permeability) are provided Table 1 [20], and the final three-dimensional model of the transformer is shown in Figure 1.

Table 1. Properties of the materials used in the simulation model.

Material	Relative Permittivity	Conductivity (S/m)	Relative Magnetic Permeability
Copper	∞	6.0×10^{7}	1
Oil-impregnated paper	3.9	1.0×10^{-14}	1
Silicon steel	∞	2.0×10^{4}	6000
Steel	∞	1.0×10^{6}	500

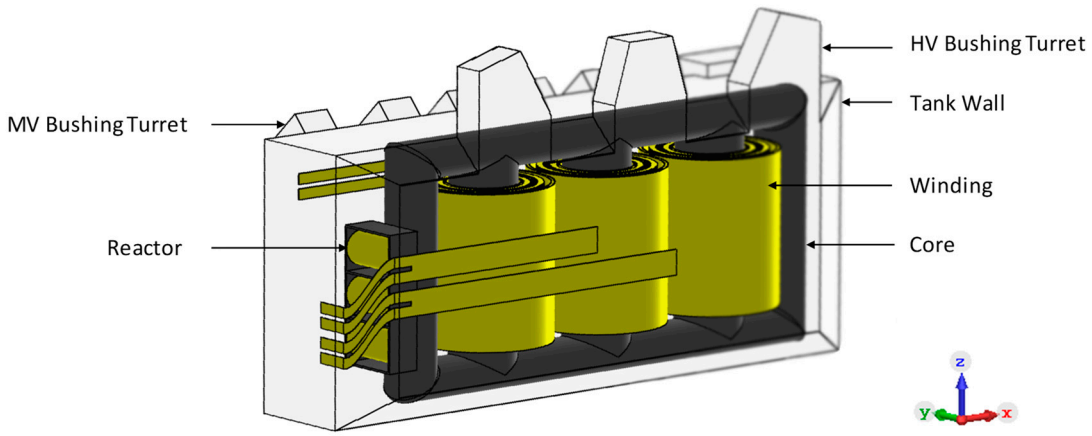

Figure 1. Three-dimensional simulation model of the transformer.

Two dielectric media were used, namely air and oil. The experiment, based on which the simulation model was validated, was carried out with air in the transformer tank. Therefore, the simulations with the sensor array were first carried out with the same medium. Thereafter, oil was used as the dielectric medium to analyze the difference between the two mediums and also because continuous UHF PD monitoring takes place when a transformer is under operation, i.e., filled with oil. The complex permittivity ε^* was used in the simulations to take into account the dispersive losses in oil. The complex permittivity is represented by Equation (1).

$$\varepsilon^* = \varepsilon' - j\epsilon'' \tag{1}$$

Here, ε' is the real component of permittivity and ε'' is the imaginary component of the permittivity. A first-order Debye model function, as shown in Equation (2), was used to obtain complex permittivity [21].

$$\varepsilon^* = \varepsilon_\infty + \frac{\varepsilon_s - \varepsilon_\infty}{1 + j\omega\tau} \tag{2}$$

Here, ω is the angular frequency, ε_∞ is the permittivity when ω approaches infinity and is set at 2.2, ε_s is the permittivity at static or low frequency and is set at 2.3, and τ is the relaxation time and is set at 1×10^{-8} s [22]. The real component of permittivity is almost frequency independent, whereas the imaginary component shows more frequency-dependent behavior, as shown in Figure 2.

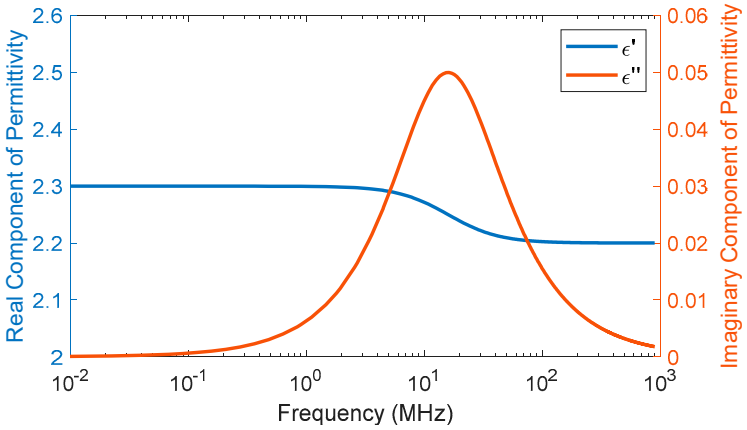

Figure 2. Frequency-dependent behavior of the permittivity of oil [22].

The setup consists of an array of UHF sensors placed on three sides of the transformer tank, namely the high voltage (HV) side, medium voltage/low voltage (MV/LV) side (because of the location of the bushing turrets of the respective windings), and the top of the tank. 12 sensors each were placed on the HV and MV/LV sides in the formation shown in Figure 3, in which 4 sensors were placed in 3 rows. Considering the topmost row on the HV side, which consists of sensors 1 to 4, sensor 1 is placed near the outer return limb of the yoke to increase the spatial distance between the parts at HV potential. Ideally, sensor 4 should have been placed in the same position on the other outer return limb. However, that is not possible in the simulation due to the construction of the tank. The non-orthogonal edges do not allow for the positioning of the ports required to simulate the sensors. Sensors 2 and 3 were placed in the gaps between the winding block of phase V and the winding blocks of the remaining two phases (U and W) to increase the spatial distance from the windings. The same configuration is used on the MV side. The sensors on the HV and MV/LV side are represented by the blue circles and squares in Figure 3, respectively.

Even though sensors positioned on the walls along the width of the transformer show similar performance for artificial PD sources at comparable distances on either of the HV or MV/LV walls, in practice, these sides are often inaccessible because of the cooling systems [17]. Therefore, it is not

convenient to install sensors in these locations, and no sensors were installed on the walls along the width of the transformer in the simulation model.

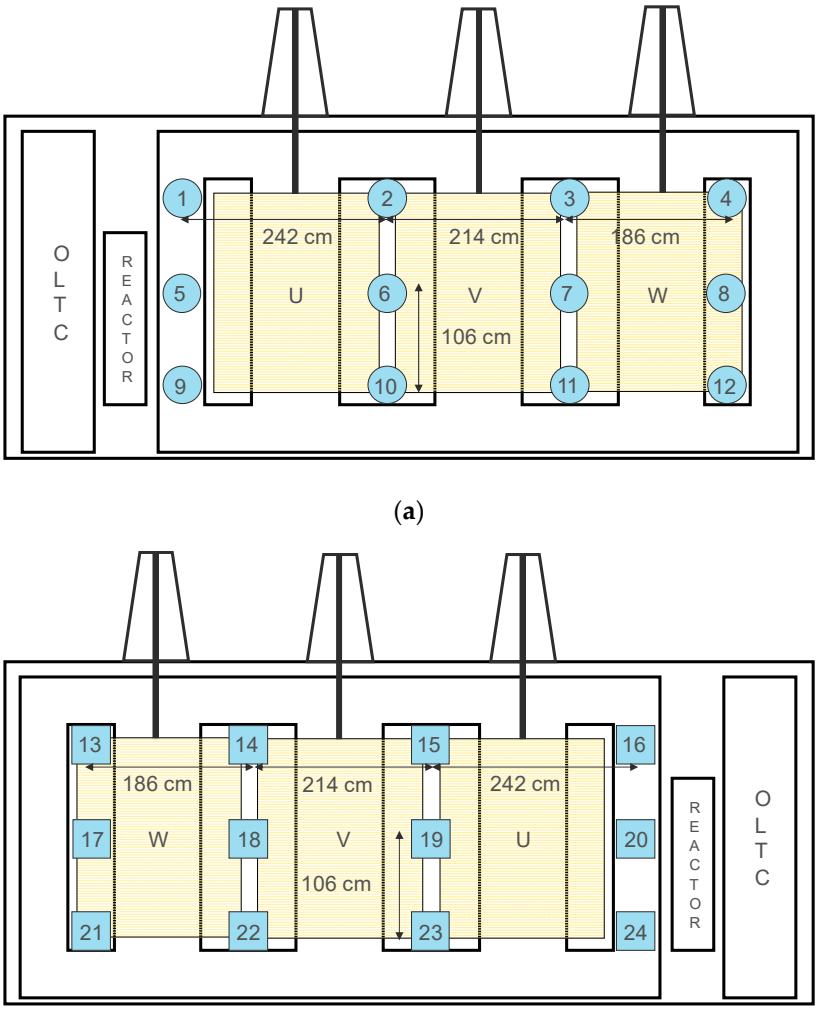

Figure 3. (**a**) Sensor placement on the high voltage (HV) side (blue circles); (**b**) sensor placement on the medium voltage/low voltage (MV/LV) side (blue squares).

On the top of the tank, the first row has only three sensors because of the presence of the LV bushings. As a result, there are 11 sensors on the top. The sensors are represented by blue triangles, and their positioning is shown in Figure 4. In total, 35 sensors were placed on the tank walls (12 each on the vertical tank walls, and 11 on the top of the tank).

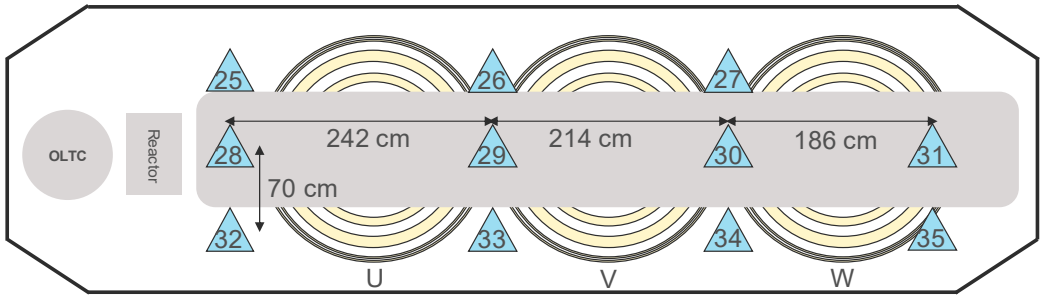

Figure 4. Sensor placement on the top of the tank (blue triangles).

The UHF sensor design is based on that of the window-type sensors [16], and the simulation model of such a sensor is shown in Figure 5. The sensor head is constructed as a conical frustum having diameters of 1 cm and 3 cm for the top and bottom of the frustum, respectively. A small cylindrical conductor is attached to the top of the sensor head, which is placed at a small distance of 0.1 cm from the inner surface of the transformer tank wall. In this gap, an S-parameter port is used to enable voltage measurement through the sensor head, which represents the signal received by the sensor. The entire arrangement is surrounded by a cylindrical plastic cover [20]. As for the artificial PD sources, 10 cm long monopole antennas are used [23,24], as shown in Figure 5. Since the monopoles are placed inside the winding, a square plate at a distance of 0.05 cm from the base of the monopole is used as the grounding plane. A voltage port is used to supply the exciting signal, i.e., the artificial PD pulse. The conducting parts of both the UHF sensors and the monopole antennas are modeled as perfect electric conductors (PEC) [20].

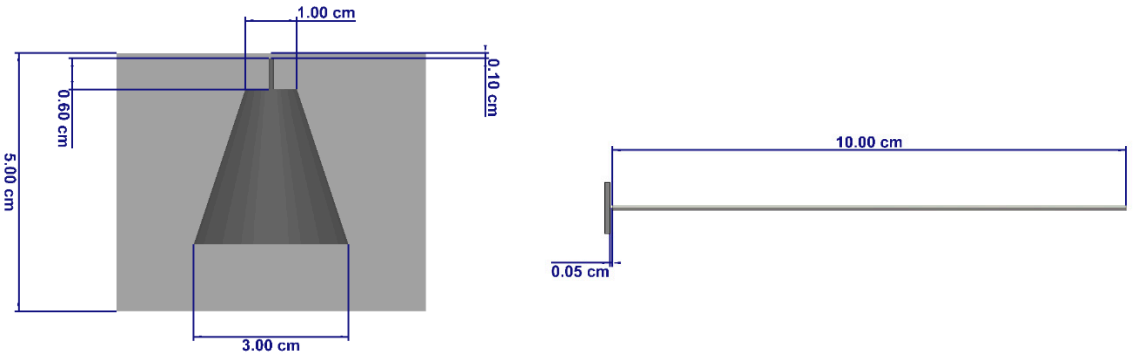

(**a**) (**b**)

Figure 5. (**a**) Design of the ultra-high frequency (UHF) sensor; (**b**) design of the monopole used as an artificial partial discharge (PD) source.

The artificial PD pulse, as shown in Figure 6, is a square wave impulse, which provides frequency content up to approximately 1 GHz, is provided as the exciting signal with a peak signal strength of approximately 60 V. This waveform and signal strength were selected to maintain equivalence between the excitation signals used in the experiment described in [17].

For meshing, a hexahedral mesh was used. Additionally, a time-domain solver is selected and used with the lowest available accuracy setting of –20 dB and simulation time of 100 ns. The frequency range for the simulation is set between 0 and 900 MHz to ensure a reasonable computation time [25]. The transformer tank acts as the boundary of the setup, as all signal propagation happens inside the closed tank.

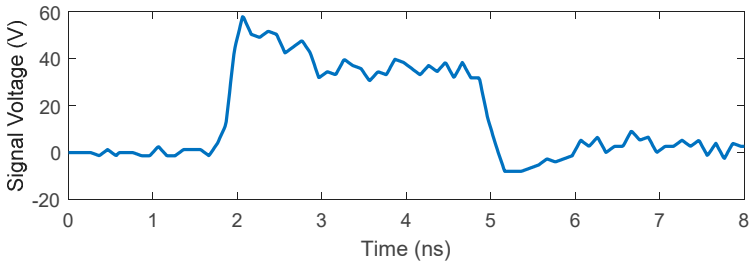

(**a**)

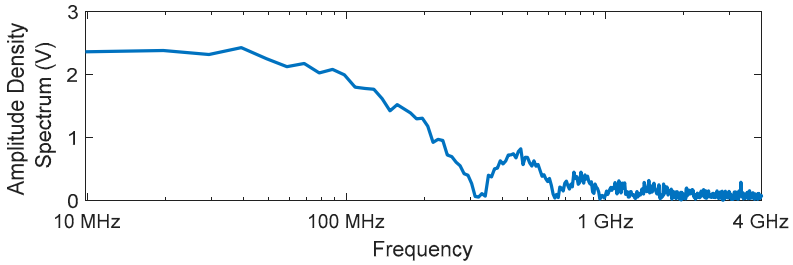

(**b**)

Figure 6. (**a**) Time-domain waveform of the artificial PD pulse; (**b**) frequency spectrum of the artificial PD pulse.

Four sources are placed in each phase in the gap between the HV and the MV windings, as represented by the red circles in Figure 7, i.e., a total of 12 sources. Concerning the depth of insertion inside the winding, the sources are exactly at the center of the winding height, as shown in Figure 8, as placing the sources near the top or bottom of the windings would skew the sensitivity analysis in favor of the sensors closest to those positions.

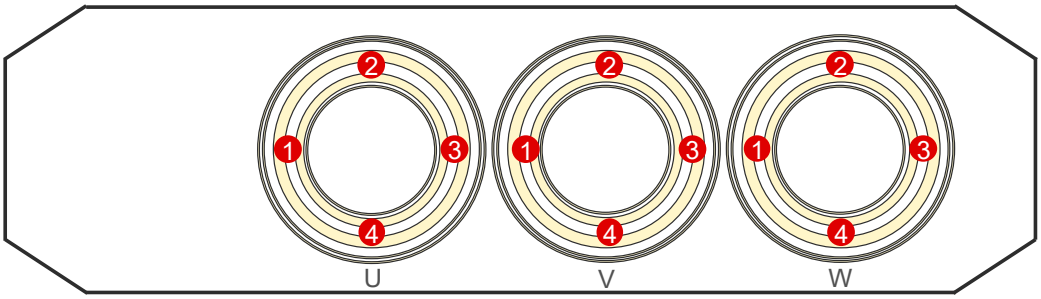

Figure 7. Location of the artificial PD sources (red circles).

3. Results

3.1. Signal Propagation and Attenuation Characteristics

Since the outer layer windings are modeled as solid cylinders [20], this simulation represents a worst-case scenario where the EM waves generated by the PD sources cannot travel through the windings. Therefore, after hitting the inner surface of the outer winding, the waves are reflected radially and axially. The axially reflected waves emerge from the top and bottom of the windings and eventually propagate through the oil space in the tank. A similar phenomenon happens with the radially reflected waves after reaching the opposite side of the windings. Figure 8 shows the direction of propagation of the waves with the red lines when the sensor is in winding block V, position 4.

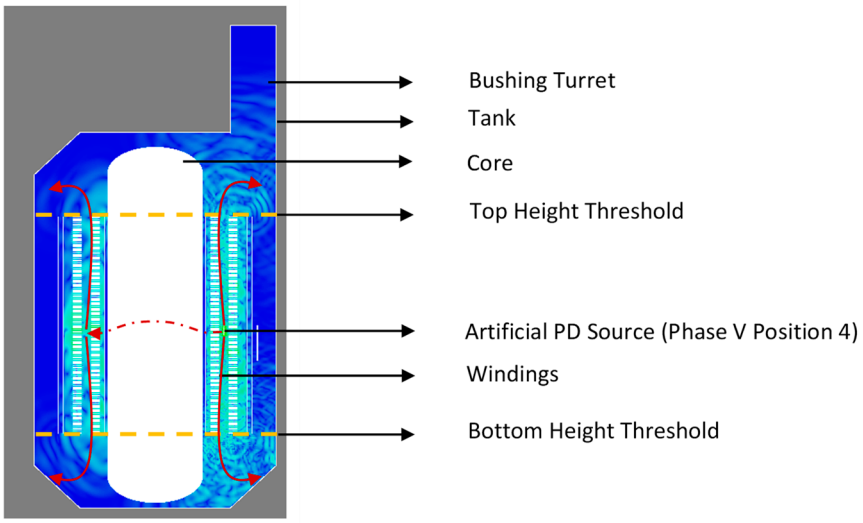

Figure 8. Propagation of electromagnetic waves from within the winding with air as the dielectric medium 6 ns after excitation (side-view).

This phenomenon has implications on the positioning of sensors in that the sensors should be ideally placed above and below the highest and lowest points of the windings, respectively because these positions are closest to where the signals emerge from the windings. The installation height thresholds are represented by the dotted yellow lines in Figure 8. The propagation path in both air and oil remains unchanged; however, the propagation velocity changes due to the change in permittivity. Hence, in air, the EM waves take approximately 6 ns to exit the winding from the top and the bottom, whereas in oil, the time is 8 ns. In air, it takes approximately 30 ns for the EM waves to cover the entirety of the tank, as shown in Figure 9, whereas in oil, it takes a little over 40 ns. The major differences between the signals received in the two media lie in the propagation times and signal attenuation. The speed of EM waves is equal to the speed of light in air. In oil with a permittivity of 2.3, the speed is approximately two-thirds of the speed in air. However, since the simulation takes into account the dispersive effects in oil, it is important to note that different frequency components of the EM wave will travel at different speeds.

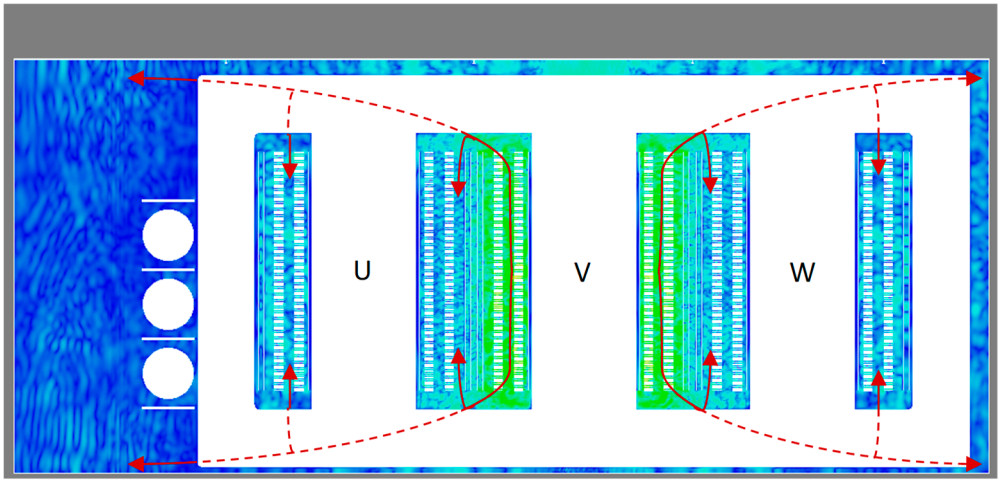

Figure 9. Electromagnetic waves present in the entirety of the tank with air as the dielectric medium 30 ns after excitation (view from HV side).

Apart from the dielectric medium, it is known that the attenuation of the UHF signals depends on the propagation distance and the propagation path. In the previously conducted experiment, since both the sending and receiving antennas were installed on the tank wall, the propagation of the EM waves was mostly in the free space of the tank and not inside the windings [17]. Since the previous

simulation setup mimicked the experimental setup [19], and since, in the present simulation setup, the propagation is first inside the winding and then in the free space, a difference in the level of attenuation between the two simulation setups should be expected. Analysis of the data from the two setups showed this assumption to be true. For example, in the previous simulation, an attenuation of –37.91 dB was measured when the sending and receiving sensors were 173 cm apart. In the present simulation, an attenuation of –66.78 dB was measured at a distance of 178.4 cm, which highlights a larger attenuation during propagation from within the winding. This difference holds true for all comparable points between the two setups.

From the symmetrical nature of the simulation setup, the performance of the "HV" and "MV/LV" sensors are expected to be similar, and for the "top" sensors, the general performance is expected to be better than the other two categories, because the propagation path from the PD source to the "top" sensors is generally shorter. Curve fitting was used for each sensor category, as shown in Figure 10, to statistically evaluate the distance-dependent attenuation for all combinations of PD sources and receiving sensors in air and oil. It should be noted that the distance represented here is the line-of-sight (a straight line) between the PD source and the receiving sensor. It does not represent the actual propagation distance. It can be observed that, as expected, the performance of the "top" sensors are indeed higher than that of the other two categories at comparable distances. However, between the "HV" and "MV/LV" sensors, there is a difference in performance with the "MV/LV" sensors performing better, contrary to expectations, which can be attributed to the difference in the size of the bushing turrets on both sides. Since the turrets are smaller on the MV/LV side of the tank, the EM waves suffer lower attenuation on this side, thus resulting in better performance of the corresponding sensors. It should be noted that all received signals are severely attenuated with respect to the strength of the input signal (60 V).

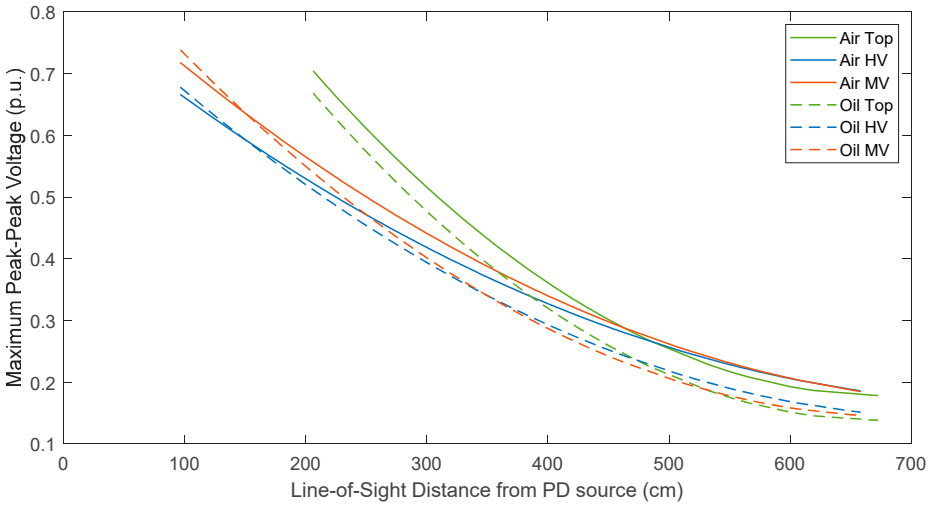

Figure 10. Attenuation of signals in oil and air for all sensor categories with increasing line-of-sight distance from PD sources.

On comparing the line-of-sight attenuation in air to that in oil, the attenuation in oil is observed to be higher at comparable distances. However, the trends observed in the sensor categories are essentially the same in both media, which indicates that similar conclusions can be drawn using simulations in both air and oil. Additionally, since the signal levels are similar, i.e., between 10 mV to 60 mV, in both media, simulations with air as the dielectric medium can be used to predict the performance in oil, since simulations using air are less resource-intensive.

3.2. Sensitivity Analysis of Different Sensor Positions

For the sensitivity analysis, each side of the transformer tank was considered, and the most sensitive sensors on each side were determined. Thereafter, the most sensitive sensors on each side

were compared to find the areas with the highest sensitivity, which were then used to propose sensor configurations for UHF PD measurement [17]. However, before the analysis was performed, certain reference values were calculated using which, the performance of the sensors was gauged. Additionally, the analysis was first performed in air and then compared with the results obtained from oil. As stated previously, the conclusions obtained in both media are essentially the same.

The sensitivity analysis is based on the attenuation of the signals. Therefore, it is necessary to classify a minimum threshold that signifies the quality of the received signals [17]. Since each simulation consists of one source and 35 receiving sensors, and since there are 12 sources, 420 signals are obtained. In order to filter the weak statistical outliers, it is decided to ignore any data point having a signal strength below one negative standard deviation from the global mean (mean signal strength of all 420 data points), which is calculated to be 16.5 mV and corresponds to an attenuation of –71.21 dB. It is found that only 75 data points lie below this threshold. The receiving sensors with the number of data points below this threshold are shown in Table 2. It can be observed that around half of the receiving sensors have no signals or only one signal below the threshold.

In general, the sources inside the winding V are well detected by almost all sensors. However, for the remaining two windings (U and W), the farthest sensors consistently receive signals below this threshold. For example, for sources in winding block W, sensors 1, 5, and 9 on the HV side and sensors 16, 20, and 24 on the MV side receive signals below the threshold. The same conclusion can be drawn for the winding U, suggesting that these windings are the limiting factors when deciding to place window sensors. Therefore, if the objective is to detect PD sources, then it is required to have at least two sensors, one near each of these windings and on opposite vertical tank walls [17].

Table 2. Number of signals detected by each sensor category that are below the threshold.

Number of Signals below Threshold	HV Sensors	MV/LV Sensors	Top Sensors
6			28
5	9		31
4	1, 4, 5, 12	13, 16, 20, 21, 24	29, 32, 35
3	8		25
2		17	
1	10	22	30
0	2, 3, 6, 7, 11	14, 15, 18, 19, 23	26, 27, 33, 34

3.2.1. HV and MV/LV Sensors

Based on the results of the experiment [17], sensors near the outer return limb of the yoke were recommended as they had the highest sensitivity and were also located away from the parts at HV potential. However, as previously mentioned, the signal propagation was mostly in the free space of the transformer. Therefore, it is necessary to identify if sensors installed at these positions are still the most sensitive when the PD sources are inside the winding. The sensors corresponding to these locations are sensors 1, 4, 5, 8, 9, and 12 on the HV side and sensors 13, 16, 17, 20, 21, and 24 on the MV/LV side. From Table 2, it can be observed that most of these sensors have four PD sources from which they receive signals that are below the threshold. As expected, these four sources correspond to the sources in the windings farthest from these sensors. For example, in the case of sensor 13, the four signals below the threshold are from sources in winding U, which is the winding farthest from the sensor. These sensor positions are most sensitive when PD occurs outside the winding, and even when the PD sources are inside the winding, at least 66.6 % of the signals are above the threshold.

For the sensors installed in the gaps between winding V and the other two windings, i.e., sensors 2, 3, 6, 7, 10 and 11 on the HV side and sensors 14, 15, 18, 19, 22, and 23, it is evident from Table 2 that most of these sensors receive signals above the threshold from all sources. Only two sensors receive one signal each that are below the threshold, and even these signals are slightly below the threshold of 16.5 mV. Therefore, these sensor positions are the most sensitive when the PD sources are inside the winding. However, more than one sensor is still required to provide complete coverage of that tank, as is evident from the results in [17].

3.2.2. Top Sensors

Similar to the sensors on the vertical walls, the sensors near the outer return limbs of the yoke, i.e., sensors 25, 28, 31, 32, and 35 suffer from the same problem of receiving signals below the threshold for PD sources that are farthest from each of the sensors. Additionally, most of the sensors installed directly above the yoke, i.e., sensors 28, 29, 30, 31, constitute the least sensitive sensors on the top of the tank. An explanation for which could be the obstruction caused by the yoke in addition to the distance from the PD sources. In fact, sensor 28 is the least sensitive sensor overall, failing to receive more than six signals above the threshold. The only sensors left are those installed in the gap between winding U and the remaining two windings that are also not installed directly above the yoke, i.e., sensors 26, 27, 33, and 34. These sensors receive signals from all PD sources above the threshold, as shown in Table 2, because of their proximity to the PD sources and the lack of obstruction from the yoke.

3.2.3. Most Sensitive Sensor Positions

From Section 3.2.1, it can be observed that sensors installed in the gaps between winding V and the other two windings have the highest sensitivity on the vertical tank walls. Similarly, from Section 3.2.2, it can be observed that the sensors in the gaps but unobstructed by the yoke are the most sensitive on the top of the tank. Overall, the "top" sensors exhibit higher sensitivity than the sensors on the vertical tank walls at comparable distances, which makes these sensors the most sensitive. The sensors with the highest sensitivity on each tank wall receive all signals above the threshold, and additionally, each of these sensors has a mean performance higher than the global mean. Therefore, it can be concluded that the highest sensitivity to PD sources inside the windings can be achieved when the sensors are installed on the tank walls in the gaps between winding V and the remaining two windings. An additional requirement for sensors installed on the vertical tank walls is that the sensors should be installed above and below the highest and the lowest points of the winding, respectively.

3.3. Proposals for Optimal Sensor Placement for PD Source Localization

As mentioned in Section 3.2, two sensors are sufficient if the aim is to detect PD sources. However, if a three-dimensional PD source localization is required, then the following requirements should be met for the placement of UHF sensors. At least four sensors are required to triangulate the PD source using time difference of arrival (TDOA) [26]. Additionally, all four sensors should not be placed on the same tank wall, and two sensors on the same tank wall should not be placed close together. Lastly, all four sensors should not form a geometrical plane [27]. However, using additional sensors can aid in PD source localization in case four sensors cannot provide enough information in the TDOA. The proposed setups for PD source localization are optimized for UHF signal sensitivity, which is also required for localization.

3.3.1. Using Most Sensitive Sensor Positions

This section discusses UHF sensor configurations in which the most sensitive positions on each side of the tank are chosen. The primary configuration consists of four sensors, with two sensors installed on the top of the tank and two sensors on the vertical tank walls. An alternate configuration also consisting of four sensors is proposed, in which all four sensors are installed on the vertical tank walls. A third optional configuration is also proposed, in which six sensors are used, with four sensors on the vertical tank walls and two on the top of the tank.

In many cases, it is easier to install and maintain sensors on the top of the tank. These sensors also perform better than the sensors on the vertical tank walls at comparable distances, as shown in Figure 10. However, installing all four sensors on the top of the tank is also not a possibility, as it would not meet the requirements for the placement of sensors [27]. Therefore, the primary configuration consists of two sensors on the top of the tank and one sensor on each vertical tank wall, i.e., four sensors in total. The two sensors on the top of the tank have to be installed in a diagonal

formation to increase the spatial distance between the sensors. Two diagonal pairs are possible, with the first diagonal sensor pair consisting of sensors 26 and 34, and the second pair consisting of sensors 27 and 33. Two sensor pairs are also defined for the sensors on the vertical tank walls to fulfill the requirements for sensor placement. The first sensor pair consists of sensors 10 and 22, and the second sensor pair consists of sensors 11 and 23. The corresponding sensor pairs should be selected to form the configuration, i.e., if the first sensor pair is selected for the "top" sensors, then the first sensor pair should be selected for the sensors on the vertical tank walls, and the same rule applies to the second sensor pairs. In Figure 11, the configuration with the second sensor pairs selected is shown. Again, the blue circles, rectangles, and triangles represent sensors placed on the HV side, MV/LV side, and the top of the tank, respectively. The lowest measured signal strength using this configuration is 18.78 mV, which is above the threshold defined in Section 3.2. This implies that the sensitivity is quite high in this configuration, even for the farthest PD sources. Additionally, the performance of the primary configuration remains similar even if the second sensor pairs are selected.

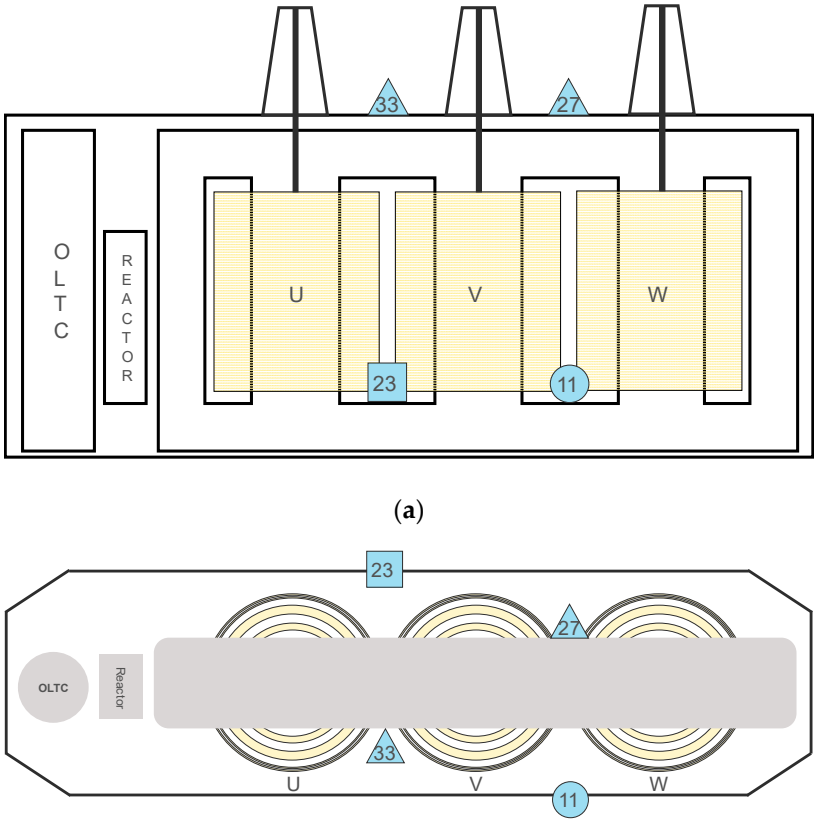

Figure 11. (**a**) Primary configuration for possible PD localization with two sensors on the top and two sensors on the vertical tank walls (view from HV side); (**b**) top view.

The alternate configuration is proposed for situations where it is not possible to install sensors on the top of the tank, in which case, all four sensors have to be installed on the vertical tank walls. Therefore, two sensors in a diagonal formation will be installed on each wall for a total of four sensors. In this configuration, a cross-diagonal arrangement using sensors on the HV and MV/LV side, similar to the one obtained from the experimental results [17], will be used to maximize the spatial distance between the sensors and to prevent the formation of a geometrical plane. The only difference being that the installed sensors are in the gaps between winding V and the remaining two windings and not near the outer return limbs of the yoke. The first diagonal sensor pair on the HV side consists of sensors 2 and 11, and the second pair consists of sensors 3 and 10. Similarly, on the MV/LV side, the first pair consists of sensors 14 and 23, and the second pair consists of sensors 15 and 22. Similar to the primary configuration, corresponding sensor pairs have to be selected, e.g., using the first sensor

pairs, the configuration consists of sensors 2, 11, 14, and 23. The lowest measured signal strength in this configuration is still above the threshold, thus signifying high sensitivity. However, the higher sensitivity of the "top" sensors is unavailable. Again, the performance remains similar even if the second sensor pairs are selected.

Optionally, more than four sensors can also be used, which can help in certain scenarios, e.g., if four sensors are unable to provide enough information in the TDOA of signals from the PD sources, then additional UHF sensors can provide additional information to aid PD source localization. In this configuration, two sensors are used on the top of the tank in a diagonal formation, and four sensors are installed on the vertical tank walls like in the alternate configuration. The sensor pairs on the "top" sensors remain unchanged from the primary configuration, whereas the sensor pairs on the vertical tank walls remain unchanged from the alternate configuration. In the configuration shown in Figure 12, the first sensor pairs on the top and the vertical tank walls are selected. The sensitivity with respect to the lowest measured signal remains unchanged from the first two configurations and remains similar if the second sensor pairs are selected.

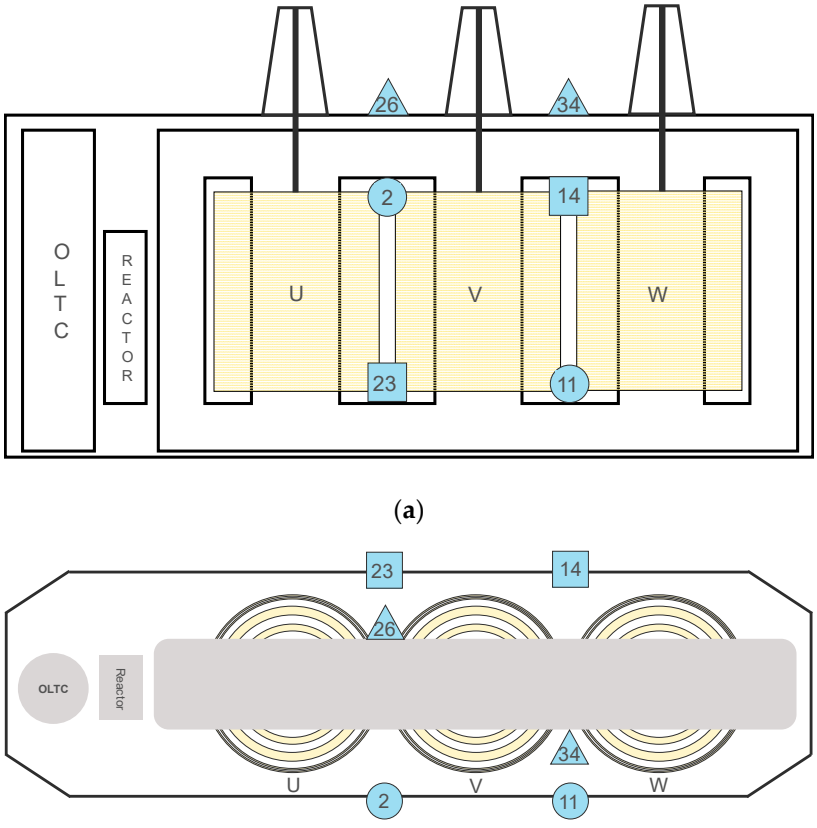

Figure 12. (**a**) Optional configuration for possible PD localization with six sensors (view from HV side); (**b**) top view.

3.3.2. Maximizing Distance from High Field Stress Regions

It is not always convenient to install sensors in the positions described in Section 3.3.1. Firstly, there may be flux shunts and other components present that may prevent installation on the vertical walls, and another factor is their proximity to the parts of the transformer at HV potential. A consideration in the placement of sensors is the electric field stress at the positions where they are installed. Since the sensors are installed in dielectric windows, a high enough electric field stress may cause PD activity at the dielectric window. A way to counteract this issue is to move the sensors away from the parts at HV potential, where the field stress is high. Therefore, the three configurations

described in this section are similar to those described in Section 3.3.1, with the key difference being that the sensors are now placed away from parts at HV potential.

For the primary configuration, there is only one diagonal sensor pair on the top of the tank because of the presence of the LV bushing, which consists of sensors 25 and 35. Therefore, sensors 9 and 21 are selected on the vertical tank walls to complete the configuration. This arrangement is shown in Figure 13. The sensitivity is reduced compared to the primary configuration discussed in Section 3.3.1. The lowest measured signals for each sensor are below the threshold and, as expected, originate from the PD sources farthest from each sensor. However, there are other sensors in the configuration that will receive signals from such sources at a signal strength above the threshold. For example, sensor 9 receives the weakest signals from PD sources in winding W, which are conversely the strongest signals measured by sensor 21.

In the alternate configuration, the first sensor pair on the HV side consists of sensors 1 and 12, and the second sensor pair consists of sensors 4 and 9. On the MV/LV side, the first pair consists of sensors 13 and 24, and the second pair consists of sensors 16 and 21. With the first sensor pairs selected, the configuration consists of sensors 1, 12, 13, and 24. The sensitivity with respect to the weakest measured signal remains unchanged from the primary configuration.

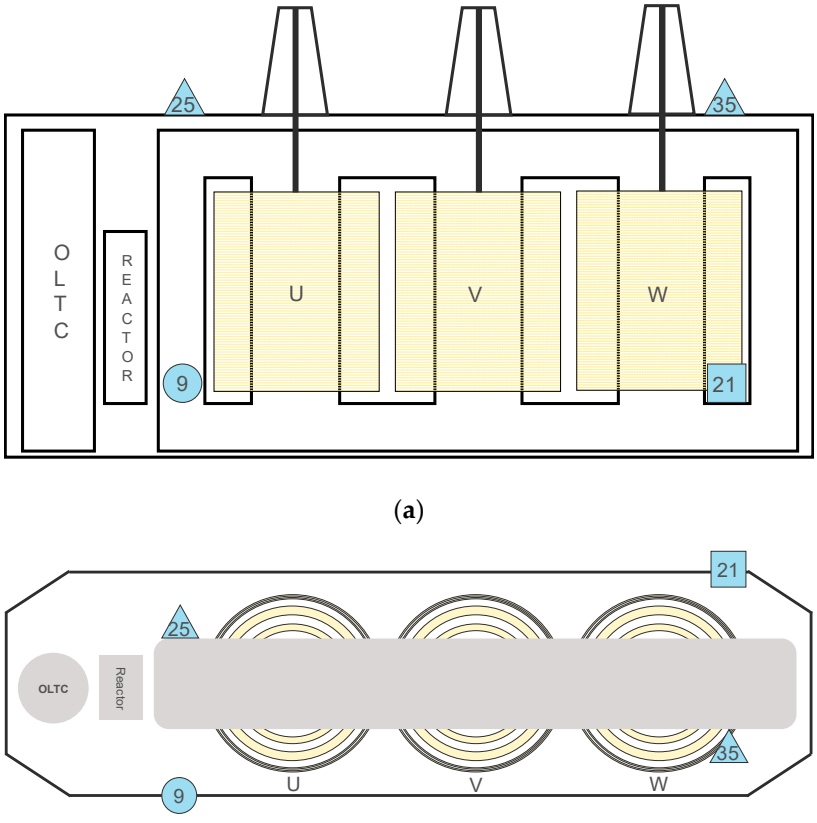

Figure 13. (**a**) Primary configuration for possible PD localization with two sensors on the top and two sensors on the vertical tank walls while maintaining a separation from high field-stress regions (view from HV side); (**b**) top view.

The optional configuration consists of sensors 25 and 35 on the top of the tank along with the first sensor pairs of the alternate configuration on the vertical tank walls. Again, six sensors are required to ensure localization of the PD source, in case four sensors provide insufficient information in the TDOA. The front and top view of this configuration are shown in Figure 14. The sensitivity with respect to the lowest measured signal strength remains unchanged from the previous configurations.

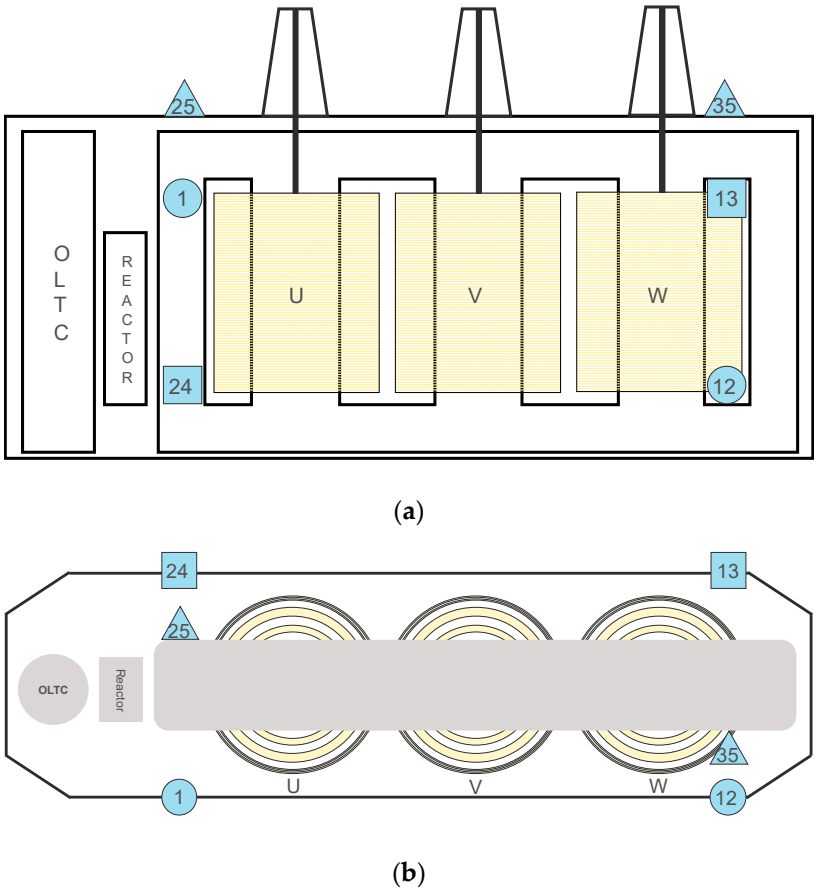

Figure 14. (**a**) Optional configuration for possible PD localization with six sensors while maintaining a separation from high field-stress regions (view from HV side); (**b**) top view.

Comparing the setups described in Sections 3.3.1 and 3.3.2, it is easily identifiable that the sensitivity is not as high when the sensors are away from the parts at HV potential and when the PD is occurring inside the windings. On average, the sensitivity with respect to the weakest measured signals is approximately 87 % higher in the configurations described in Section 3.3.1 when compared to the current configurations. However, as discussed previously, it is not always easy to install sensors in the most sensitive positions, and the high electric field stress is a concern. As a rule of thumb, it is preferable to install sensors at a specified minimum distance from the windings to prevent PD activity at the dielectric windows. The minimum installation distances of UHF sensors from windings of different rated voltages are provided in Table 3 [28].

Table 3. Minimum spacing of UHF sensors from windings of different voltage ratings.

Rating (kV)	Minimum Spacing (m)
420	1.5
230	1
130	0.8

It is quite evident that the configurations described in Section 3.3.2 are more likely to meet these requirements. Additionally, it was found from the experiment that sensors installed near the outer return limbs of the yoke were the most sensitive when PDs occurred outside the winding because of fewer obstacles around these positions [17]. When the aforementioned points are taken into account, the primary configuration recommended in Section 3.3.2, and shown in Figure 13, is found to balance the distance of the UHF sensors from the parts at HV potential while providing sufficient sensitivity to PD activity inside the windings and thus, is the most practical configuration.

4. Conclusions

In this contribution, simulations were carried out using a validated model of a three-phase 300 MVA, 420 kV power transformer, in which artificial PD sources were placed inside the winding, to determine the positions on the tank wall where the UHF sensors could measure PD pulses from inside the winding with the highest sensitivity. A statistical threshold was used to filter the weak signals, and it was found that the weakest signals were always received from the sources in the winding farthest from a UHF sensor. Only the sources inside the middle winding were measured above the threshold by all sensors, which implied that the other two windings were the limiting factors while placing sensors. Therefore, at least two UHF sensors are required if the goal is to detect PD sources.

A sensitivity analysis was performed to identify the most sensitive sensors on each tank wall, based on which sensor configurations for PD source localization were proposed with two different approaches. The first was simply using the most sensitive sensor positions, whereas the second approach took into account the proximity of the sensors from the parts at HV potential. It was recommended to use the latter approach because of the minimum spacing requirements of the UHF sensors from parts at HV potential. The basic configuration consists of four sensors placed near the outer return limbs of the yoke, with two sensors on the top of the tank and two sensors on the vertical tank walls. However, to ensure PD source localization, six sensors are recommended, with two sensors on the top of the tank and four sensors on the vertical tank walls.

Additionally, the difference in propagation and attenuation in two mediums (oil and air) was studied and found to be negligible, and the sensitivity analysis provided the same conclusions in both mediums. Therefore, a simulation in air can be used to predict the performance in oil.

5. Outlook

The most important aspect that requires further study is the attenuation with respect to actual propagation distance and not the line-of-sight distance, which is a simplification of the complex propagation path inside the transformer. Additionally, the sensitivity analysis will be performed in transformers of varying ratings to determine if the conclusions drawn in this contribution hold true in various scenarios.

Author Contributions: Conceptualization, C.P.B. and S.T.; investigation, C.P.B., M.B., S.T., and M.S.; data curation, C.P.B.; writing—original draft preparation, C.P.B.; writing—review and editing, C.P.B., M.B., S.T., and M.S.; visualization, C.P.B.; supervision, S.T. All authors have read and agreed to the published version of the manuscript.

Funding: This research received no external funding.

Conflicts of Interest: The authors declare no conflict of interest.

References

1. International Electrotechnical Commission. *IEC 62478 High voltage test techniques –Measurement of partial discharges by electromagnetic and acoustic methods;* IEC: Geneva, Switzerland, 2016, ISBN 978-2-8322-3560-7.
2. Chai, H.; Phung, B.T.; Mitchell, S. Application of UHF Sensors in Power System Equipment for Partial Discharge Detection: A Review. *Sensors* **2019**, *19*, doi:10.3390/s19051029.
3. Tenbohlen, S.; Beltle, M.; Siegel, M. PD monitoring of power transformers by UHF sensors. In Proceedings of the 2017 International Symposium on Electrical Insulating Materials (ISEIM), Toyohashi, 11–15 September 2017; pp. 303–306, ISBN 978-4-88686-099-6.
4. Dukanac, D. Application of UHF method for partial discharge source location in power transformers. *IEEE Trans. Dielect. Electr. Insul.* **2018**, *25*, 2266–2278, doi:10.1109/TDEI.2018.006996.
5. Romano, P.; Imburgia, A.; Ala, G. Partial Discharge Detection Using a Spherical Electromagnetic Sensor. *Sensors* **2019**, *19*, doi:10.3390/s19051014.
6. Nobrega, L.A.M.M.; Xavier, G.V.R.; Aquino, M.V.D.; Serres, A.J.R.; Albuquerque, C.C.R.; Costa, E.G. Design and Development of a Bio-Inspired UHF Sensor for Partial Discharge Detection in Power Transformers. *Sensors* **2019**, *19*, doi:10.3390/s19030653.

7. Zachariades, C.; Shuttleworth, R.; Giussani, R. A Dual-Slot Barrier Sensor for Partial Discharge Detection in Gas-Insulated Equipment. *IEEE Sensors J.* **2019**, 1, doi:10.1109/JSEN.2019.2943625.
8. Li, J.; Han, X.; Liu, Z.; Yao, X. A Novel GIS Partial Discharge Detection Sensor With Integrated Optical and UHF Methods. *IEEE Trans. Power Deliv.* **2018**, *33*, 2047–2049, doi:10.1109/TPWRD.2016.2635382.
9. CIGRÉ. *Guidelines for partial discharge detection using conventional (IEC 60270) and unconventional methods;* CIGRÉ: Paris, 2016, ISBN 978-2-85873-365-1.
10. Nobrega, L.; Costa, E.; Serres, A.; Xavier, G.; Aquino, M. UHF Partial Discharge Location in PowerTransformers via Solution of the MaxwellEquations in a Computational Environment. *Sensors* **2019**, *19*, doi:10.3390/s19153435.
11. Xue, N.; Yang, J.; Shen, D.; Xu, P.; Yang, K.; Zhuo, Z.; Zhang, L.; Zhang, J. The Location of Partial Discharge Sources Inside Power Transformers Based on TDOA Database with UHF Sensors. *IEEE Access* **2019**, *7*, 146732–146744, doi:10.1109/ACCESS.2019.2945893.
12. Siegel, M.; Coenen, S.; Beltle, M.; Tenbohlen, S.; Weber, M.; Fehlmann, P.; Hoek, S.M.; Kempf, U.; Schwarz, R.; Linn, T.; et al. Calibration Proposal for UHF Partial Discharge Measurements at Power Transformers. *Energies* **2019**, *12*, 3058, doi:10.3390/en12163058.
13. Siegel, M.; Tenbohlen, S. Calibration of UHF Partial Discharge Measurement for Power Transformers and a Comparison to the Calibration of Electrical PD Measurement. In Proceedings of the IEEE Electrical Insulation Conference, Montréal, Canada, 19–22 June 2016.
14. International Electrotechnical Commission. *IEC 60270 High-voltage test techniques: partial discharge measurements;* IEC: Geneva, Switzerland, 2000.
15. Mirzaei, H.R.; Akbari, A.; Zanjani, M.; Miralikhani, K.; Gockenbach, E.; Borsi, H. Investigating suitable positions in power transformers for installing UHF antennas for partial discharge localization. In Proceedings of the 2012 IEEE International Conference on Condition Monitoring and Diagnosis (CMD), Bali, Indonesia, 23–27 September 2012; pp. 625–628, ISBN 978-1-4673-1020-8.
16. Siegel, M.; Beltle, M.; Tenbohlen, S.; Coenen, S. Application of UHF sensors for PD measurement at power transformers. *IEEE Trans. Dielect. Electr. Insul.* **2017**, *24*, 331–339, doi:10.1109/TDEI.2016.005913.
17. Beura, C.P.; Beltle, M.; Tenbohlen, S. Positioning of UHF PD Sensors on Power Transformers Based on the Attenuation of UHF Signals. *IEEE Trans. Power Delivery* **2019**, *34*, 1520–1529, doi:10.1109/TPWRD.2019.2909588.
18. Giglia, G.; Ala, G.; Castiglia, V.; Imburgia, A.; Miceli, R.; Rizzo, G.; Romano, P.; Schettino, G.; Viola, F. Electromagnetic Full-Wave Simulation of Partial Discharge Detection in High Voltage AC Cables. In Proceedings of the 2019 IEEE 5th International forum on Research and Technology for Society and Industry (RTSI), Florence, Italy, 9–12 September 2019; pp. 166–171, ISBN 978-1-7281-3815-2.
19. Beura, C.P.; Beltle, M.; Tenbohlen, S. Attenuation of UHF Signals in a 420 kV Power Transformer Based on Experiments and Simulation. In *Proceedings of the 21st International Symposium on High Voltage Engineering*; Németh, B., Ed.; Springer International Publishing: Cham, 2020; pp. 1276–1285, ISBN 978-3-030-31679-2.
20. Umemoto, T.; Tenbohlen, S. Novel Simulation Technique of Electromagnetic Wave Propagation in the Ultra High Frequency Range within Power Transformers. *Sensors* **2018**, *18*, doi:10.3390/s18124236.
21. Zheng, Y.-m.; Wang, Z.-j. Study on broadband loss characteristics of oil-immersed papers for fast transient modeling of power transformer. *IEEE Trans. Dielect. Electr. Insul.* **2013**, *20*, 564–570, doi:10.1109/TDEI.2013.6508760.
22. Umemoto, T.; Tenbohlen, S. Validation of Simulated UHF Electromagnetic Wave Propagation in Power Transformers by Time and Frequency Domain Measurements. In Proceedings of the 2018 IEEE International Conference on High Voltage Engineering and Application (ICHVE), ATHENS, Greece, 10–13 September 2018; pp. 1–4, ISBN 978-1-5386-5086-8.
23. Coenen, S.; Tenbohlen, S.; Markalous, S.M.; Strehl, T. Attenuation of UHF signals regarding the sensitivity verification for UHF PD measurements on power transformers. In Proceedings of the 2008 International Conference on Condition Monitoring and Diagnosis, Beijing, China, 21–24 April 2008; pp. 1036–1039, ISBN 978-1-4244-1621-9.
24. Albarracín, R.; Ardila-Rey, J.A.; Mas'ud, A.A. On the Use of Monopole Antennas for Determining the Effect of the Enclosure of a Power Transformer Tank in Partial Discharges Electromagnetic Propagation. *Sensors* **2016**, *16*, 148, doi:10.3390/s16020148.

25. Du, J.; Chen, W.; Cui, L.; Zhang, Z.; Tenbohlen, S. Investigation on the propagation characteristics of PD-induced electromagnetic waves in an actual 110 kV power transformer and its simulation results. *IEEE Trans. Dielect. Electr. Insul.* **2018**, *25*, 1941–1948, doi:10.1109/TDEI.2018.007336.
26. Markalous, S.M.; Tenbohlen, S.; Feser, K. New robust non-iterative algorithms for acoustic PD-localization in oil/paper-insulated transformers. In Proceedings of the 14th International Symposium on High Voltage Engineering, ISH 2005, Beijing, China, 25–28 August 2005; Guan, Z., Ed.; Tsinghua Univ. Press: Beijing, 2005; p. 29, ISBN 9787302015819.
27. Mirzaei, H.; Akbari, A.; Gockenbach, E.; Miralikhani, K. Advancing new techniques for UHF PDdetection and localization in the power transformers in the factory tests. *IEEE Trans. Dielect. Electr. Insul.* **2015**, *22*, 448–455, doi:10.1109/TDEI.2014.004249.
28. Tenbohlen, S.; Beura C. P.; Beltle, M.; Siegel, M. UHF Sensor Placement on Power Transformers for PD Monitoring. In Proceedings of the CIGRE Colloquium SCA2/SCB2/SCD1, New Delhi, India, 21–22 November 2019.